ELSEVIER

Thermochimica Acta 359 (2000) 43–54

thermochimica acta

www.elsevier.com/locate/tca

Temperature modulated differential scanning calorimetry: on system linearity and the effect of kinetic events on the observed sample specific heat

S.X. Xu[a,*], Y. Li[a], Y.P. Feng[b]

[a]*Department of Materials Science, Faculty of Science, National University of Singapore, Lower Kent Ridge Road, Singapore 119260, Singapore*

[b]*Department of Physics, National University of Singapore, Singapore 119260, Singapore*

Received 10 January 2000; received in revised form 3 March 2000; accepted 6 March 2000

Abstract

In this paper, the effect of system linearity and kinetic events on heat capacity measurement by temperature modulated differential scanning calorimetry (TMDSC) is analyzed based on the thermal conduction differential equations that have been linearized assuming small kinetic perturbations. Numerical simulation of a first order reaction is used to demonstrate the importance of system linearity and the selection of experimental parameters. Experimental results of specific heat capacity determinations during crystallization of an amorphous alloy were presented.

Keywords: TMDSC; Linearity; Specific heat; Heat capacity

1. Introduction

Differential scanning calorimetry (DSC) has been used for a long time in the study of materials thermal properties and kinetic events. In 1993, temperature modulated differential scanning calorimetry (TMDSC) was introduced as a further development of conventional DSC in which a cyclic temperature modulation is superimposed on a linear or isothermal heating program [1]. There is currently a large number of research papers concerning the application of TMDSC to issues such as the measurement of heat capacity, thermal conductivity, glass transitions, curing, crystallization and melting, etc. [2–11]. TMDSC combines the benefits of a slow underlying scanning rate which will give a better temperature resolution and fast instantaneous heating rate (by the temperature modulation) that can result in a high sensitivity. It has been shown that this technique is capable of separating non-reversing processes such as the glass transition from entropy recovery, cold crystallization or the reaction heat during a curing from that of reversing ones. Also, it is believed that TMDSC has improved accuracy and faster experimental procedure compared with conventional DSC.

The fundamental analyzing method, namely the Fourier transform used in TMDSC, is based on linear response theory, which has a stringent requirement on both the TMDSC test system and the kinetic reaction itself (if any). The first order harmonics of heat flow and sample temperature are utilized to calculate the specific heat and phase angle. If experi-

* Corresponding author. Fax: +65-776-3604.
E-mail address: scip7317@nus.edu.sg (S.X. Xu)

0040-6031/00/$ – see front matter
PII: S0040-6031(00)00491-3

mental conditions are not selected properly or the system response deviates from the equilibrium states by the kinetic events, the obtained result could be far from the real situation and may lead to erroneous conclusions.

In this paper, both analytical and numerical solutions are adopted to demonstrate the importance of linearity in TMDSC. Experimental results conducted with an amorphous alloy are also given to show these effects.

2. TMDSC theory

In the following sections, the thermal analysis is based on a typical heat flux type TMDSC instrument. For ideal TMDSC test equipment, where the thermal conductance between the heating block and the reference or sample is K, the temperature gradient inside the sample and the heat exchange with the purge gas or by radiation are ignored. The following general differential equations can be obtained [12,13]:

$$C_r\left(\frac{d\Delta T}{dt}\right) + K\Delta T = C_s'\left(\frac{dT_s}{dt}\right) \tag{1}$$

where $C_s' = C_s - C_r$, which is the heat capacity of the sample, $\Delta T = T_r - T_s$ the sample and reference temperature difference, T_r the reference temperature, T_s the sample temperature, C_s the heat capacity of sample plus sealing pan, C_r heat capacity of reference pan (assuming the sample pan is identical to the reference pan) and t is the time.

If there is a kinetic event $f(t, T)$ that depends on both time and temperature on the sample side, then Eq. (1) becomes

$$C_r\left(\frac{d\Delta T}{dt}\right) + K\Delta T = C_s'\left(\frac{dT_s}{dt}\right) + f(t, T_s) \tag{2}$$

In a TMDSC device, the heating block is modulated so that the sample temperature follows a sinusoidal pattern that is superimposed on a linear heating signal even in the presence of a kinetic event. There are situations in which the sample temperature does not follow the modulation temperature at all (for example, during the melting of pure metals), hence these arguments will not apply. The sample temperature T_s is given by

$$T_s = T_0 + qt + A_{T_s}\sin(\omega t) \tag{3}$$

where T_0 is the initial temperature, q the underlying linear heating rate, A_{T_s} the sample temperature amplitude and ω the modulation angular frequency.

By inserting Eq. (3) into Eq. (2), one obtains

$$C_r\left(\frac{d\Delta T}{dt}\right) + K\Delta T = C_s'(q + A_{T_s}\omega\cos(\omega t)) + f(t, T_0 + qt + A_{T_s}\sin(\omega t)) \tag{4}$$

As can be seen from above, although the kinetic event $f(t, T)$ contains both time and temperature as its variables, these two variables are linked together by the modulation Eq. (3), i.e., $f(t, T)$ is literally turned into a single variable function. If the temperature modulation amplitude is very small, then $f(t, T_0 + qt + A_{T_s}\sin(\omega t))$ could be expressed by its first order approximation

$$f(t, T_0 + qt + A_{T_s}\sin(\omega t)) \approx f(t, T_0 + qt) + f_T'(t, T_0 + qt)A_{T_s}\sin(\omega t) \tag{5}$$

where the f_T' is the first order temperature derivative.

It is impossible or very difficult to get a round solution to Eq. (4) under most situations. To obtain an approximate analytical solution, we need to further linearize the kinetic function $f(t, T)$, again assuming that $f(t, T)$ takes a relatively long time to complete so that both $f(t, T_0+qt)$ and $f_T'(t, T_0 + qt)$ changes very little during one or even more modulation cycles. Their functions can then be roughly treated as two 'constants' in Eq. (5), and if the underlying heating rate is very slow, for example, a few degrees per minute or less, which is a typical experimental condition, also the sample heat capacity essentially remains constant in the whole process. Based on these assumptions, Eq. (4) becomes a linear differential expression. We can obtain the cyclic part of the general solution as below:

$$\Delta T_{cyclic} = \frac{A_{T_s}}{\sqrt{K^2 + \omega^2 C_r^2}}(C_s'\omega\cos(\omega t + \varphi) + f_T'(t, T_0 + qt)\sin(\omega t + \varphi)) \tag{6a}$$

where the phase angle between sample heating rate and the temperature difference is $\varphi = \tan^{-1}(-\omega C_r/K)$. This phase angle exists even without the presence of the kinetic event. Because f_T' is assumed to be almost a

constant in each modulation cycle, Eq. (6a) can be further compacted as

$$\Delta T_{\text{cyclic}} = \frac{A_{T_s} C'_s}{\sqrt{(K/\omega)^2 + C_r^2}} \times \left(\cos(\omega t + \varphi) + \frac{f'_T}{C'_s \omega}\sin(\omega t + \varphi)\right) = \frac{A_{T_s} C'_s}{\sqrt{(K/\omega)^2 + C_r^2}} \sqrt{1 + \left(\frac{f'_T}{C'_s \omega}\right)^2} \times \cos(\omega t + \varphi - \delta) \quad (6b)$$

where the extra phase angle caused by the kinetic event is δ and

$$\cos(\delta) = \frac{1}{\sqrt{1 + (f'_T/C'_s\omega)^2}} \quad (6c)$$

$$\sin(\delta) = \frac{f'_T/C'_s\omega}{\sqrt{1 + (f'_T/C'_s\omega)^2}} \quad (6d)$$

In Eq. (6a), the temperature difference between the sample and reference is governed by two components. One is heat capacity related, because this is the so called non-cooperative atomic motion that has a relaxation time in the order of 10^{-13} s [14]. This is much faster then the temperature modulation frequency, thus, the atomic motion can always instantaneously follow this external modulation and this part is commonly known as the reversing component. The second part is contributed by the temperature sensitivity of the kinetic event, such as a glass transition in a polymer, corresponding to the large molecular motions. The relaxation time of this kind of event could match that of the temperature modulation or be even longer.

In practice, the cyclic part (first harmonic) can be extracted from the heat flow signal via discrete Fourier transform. The observed sample heat capacity C'_{s_m} can be obtained from the heat flow and sample temperature amplitude [15]

$$C'_{s_m} = \frac{A_{\Delta T}}{A_{T_s}}\left(\frac{K}{\omega}\right) \quad (7)$$

where $A_{\Delta T}$ is the amplitude of the sample/reference temperature difference.

From Eq. (6a), it is easy to see that, if the kinetic event $f(t, T)=0$, sample heat capacity will be

$$C'_s = \frac{A_{\Delta T}}{A_{T_s}}\left(\frac{K}{\omega}\right)\sqrt{1 + (C_r\omega/K)^2} \quad (8)$$

where $A_{\Delta T} = A_{T_s} C'_s \omega/(K^2 + C_r^2\omega^2)^{1/2}$.

Compared with Eq. (7), in this case, there is one more item in Eq. (8) which is considered to be the calibration factor that can obtained by measuring a standard sample with known specific heat properties, usually sapphire. It is noticed that this calibration factor will be affected by the temperature modulation frequency, the system thermal constant and the reference material heat capacity in this simplified model. (Actually, factors that could contribute to its value also include purge gas convection, thermal contact resistance between pan and TMDSC cell and the actual structure of the cell itself, to name just a few. These will affect the heat conduction path thermal properties of the TMDSC cell as well.) According to Eq. (8), the sample heat capacity can be obtained after proper calibration is performed.

When there is a kinetic even $f(t, T)$, which does not exist for the inert calibration material, however, the measured sample heat capacity will be determined by both the sample heat capacity and the kinetic heat released, which can be represented as below:

$$|C_p*| = \frac{A_{\Delta T}}{A_{T_s}}\left(\frac{K}{\omega}\right)\sqrt{1 + \left(\frac{C_r\omega}{K}\right)^2}\sqrt{1 + \left(\frac{f'_T}{C'_s\omega}\right)^2} \quad (9a)$$

The above heat capacity is also called the complex heat capacity. With this complex heat capacity and Eqs. (6c), (6d) and (8), one can get the reversing (also called 'in-phase') and non-reversing (called 'out of phase') heat capacity separately as

$$C'_s = |C_p*|\cos(\delta) \quad (9b)$$

$$\frac{f'_T}{\omega} = |C_p*|\sin(\delta) \quad (9c)$$

however, it should be noted that, the concept of complex heat capacity is still controversial [16,17], as part of the observed non-reversing heat capacity can come from the lack of sufficient heat diffusion in some

low heat conductive materials such as polymers (e.g. PET's thermal conductivity is only 1/1000 that of aluminum), wood, glass and fiber, etc. These materials indeed can have significant thermal gradient inside thus will introduce extra phase lag and hence influence the test results.

The practical problem is to find the phase angle introduced by the kinetic event alone, which needs an approach to filtering out the phase lag caused by the pure thermal transfer properties from the total phase angle. Reading and Luyt suggested a base line method, which is realized by subtracting an interpolated straight line between the start and end point of the kinetic transition [18]. Weyer et al. [19] proposed another method that uses the C_p curve to deduce a fitting baseline to correct the phase angle. Nevertheless, linearity still plays an important role in phase angle compensation. For without this basic pre-condition, Eq. (6a) will result in unpredictable error to the solution of Eq. (4).

Apparently, in Eq. (9a), the sample heat capacity C'_s itself is involved in determining the result, this one can be troubling because it is right the item we want to measure. Although increasing the modulation frequency can lower its effect on the measured heat capacity, the available modulation frequency typically is restricted to only 0.01–0.1/s due to system thermal inertial, which is much narrower than that in other dynamic methods such as DMA. This makes TMDSC not very suitable in quantitative analysis under certain situations. However, as long as the kinetic event and modulation parameter selection satisfy the expression

$$\left(\frac{f'_T}{C'_s\omega}\right)^2 \max \ll 1 \tag{10}$$

the reversing heat flow can still be separated from the total heat flow signals with relatively small errors. This is where TMDSC differs from conventional DSC. Sometimes, the left hand side of Eq. (10) is not small compared to 1 and significant deviation in the measured heat capacity can develop. This can be one of the sources of incorrect explanation or quantification of reversing and non reversing part.

From the above analysis, it can be seen that the key to successful deconvolution of heat capacity is the system linearity, which comprises the instrument linearity and the kinetic event linearity (small and effectively constant f'_T). That is, for a given overall system function $F(x)$, it should satisfy $F(a+b)=F(a)+F(b)$ and $F(kx)=kF(x)$. The system can then be described by linear differential equations as above. Any kinetic event added to the right hand side of Eq. (4) that meet this condition will have its corresponding linear response superimposed on that caused by sample heat capacity C'_s, hence the Fourier transform that is applicable to linear response system is applicable here. Besides, for a complete deconvolution that takes into account the extra phase angle caused by the kinetic event, from Eqs. (6b), (6c) and (9b), (9c), the key issues are still the 'small perturbation' and system linearity. Obviously, if linearity is not good enough due to improper experimental parameter selection, or the kinetic event itself, all the above equations do not hold true and the Fourier transform will produce mathematical artifacts leading to wrong conclusions. Below, a first order chemical reaction solved numerically is used to demonstrate this.

2.1. Simulated case study, a first order chemical reaction

Assuming the kinetic event is a first order decomposition, which takes the typical Arrhenius form

$$\frac{dC}{dt} = AC\exp\left(-\frac{E_a}{RT}\right) \tag{11}$$

where C is the concentration of the reaction agent, A the reaction constant, E_a the activation energy, R the gas constant and T the temperature. From Eq. (11), one obtains

$$C = C_0\exp\left(\int_0^t A\exp\left(-\frac{E_a}{RT}\right)dt\right) \tag{12}$$

where C_0 is the initial concentration of the decomposing agent.

Then the associated kinetic heat flow $f(t, T)$ generated by the decomposition is

$$f(t,T) = \Delta H\, mAC_0\exp\left(\int_0^t A\exp\left(-\frac{E_a}{RT}\right)dt\right) \times \exp\left(-\frac{E_a}{RT}\right) \tag{13}$$

In Eq. (13), ΔH is the total reaction heat per unit mass and m the sample size.

With a linear underlying heating rate $T=T+qt$, it can be derived that

$$f'_T = \Delta H\, m \frac{A}{q} C_0 \exp\left(\int_0^t A \exp\left(-\frac{E_a}{RT}\right) dt\right) \times \exp\left(-\frac{E_a}{RT}\right)\left(\frac{E_a q}{RT^2} + A \exp\left(-\frac{E_a}{RT}\right)\right) = f(t,T)\frac{(E_a q/RT^2) + A\exp(-E_a/RT)}{q} \quad (14)$$

Eqs. (15) and (16) are the differential equations used in the finite difference numerical simulation. Simulation parameters are given in Table 1. For the sake of simplicity, it is assumed that the sample specific heat capacity keeps constant during the whole process.

$$K(T_b - T_s) = (C'_s + C_r)\left(\frac{dT_s}{dt}\right) + f(t,T) \quad (15)$$

$$K(T_b - T_r) = C_r\left(\frac{dT_r}{dt}\right) \quad (16)$$

where T_b is the heating block temperature and the rest of the symbols are defined in Eqs. (1) and (2).

A sliding Fourier transform window with the same width as the corresponding modulation period (10, 100 and 1000 s, respectively) is adopted. The plotted total heat flow, reversing and non-reversing heat flow curves are a sliding average over the transform window. Figs. 1–6 are the TMDSC simulation results with this first order decomposition.

Lissajous figures (heating rate dT_s/dt versus instantaneous heat flow instead of the sliding average) are used as a visual criteria to demonstrate the system linearity. The relationship between the separability of reversing heat flow and kinetic heat flow can be seen clearly in this case.

Table 1
Finite difference numerical simulation

Simulation parameters	
Heating block modulation amplitude (K)	0.2
Underlying heating rate q (K/min)	3
Temperature modulation period (s)	10–1000
Sample heat capacity C'_s, (J/K)	0.004
Reference heat capacity C_r (J/K)	0.0228
TMDSC system thermal conductance K (W/K)	0.01
Decomposition reaction constant A (s^{-1})	2×10^8
Activation energy E_a (J/mol)	8.314×10^4
Reaction heat per unit mass ΔH (J/g)	75
Sample mass M (g)	0.02
Initial temperature T_0 (°C)	30
Initial reaction agent concentration C_0	0.95
Gas constant R (J/mol K)	8.314

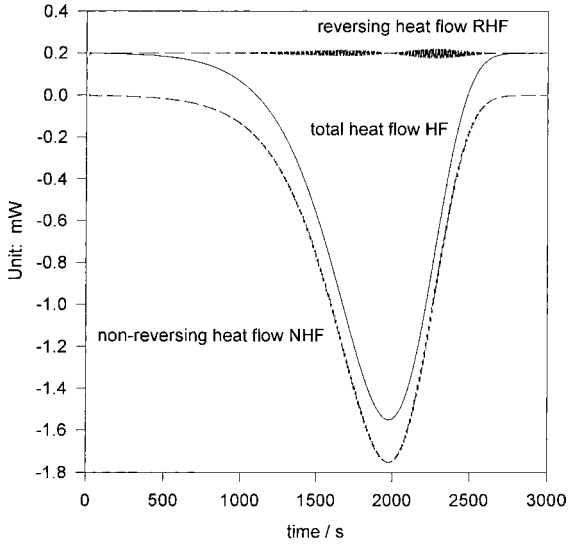

Fig. 1. Simulated total heat flow, reversing heat flow and non-reversing heat flow. Period=10 s, modulation amplitude=0.2 K and underlying heating rate=3 K/min.

In Fig. 1, the temperature modulation period is 10 s, which is the fastest among the three simulations shown

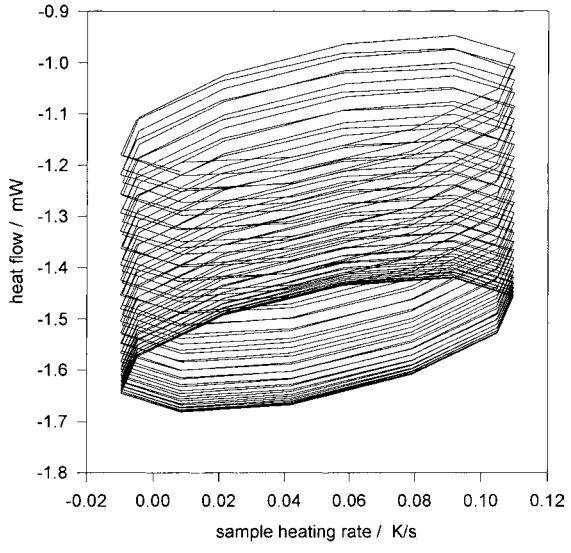

Fig. 2. Simulated Lissajous figure. Period=10 s, modulation amplitude=0.2 K and underlying heating rate=3 K/min.

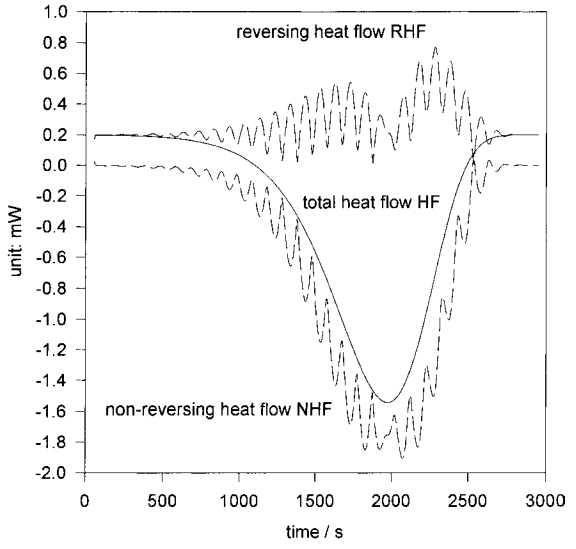

Fig. 3. Simulated total heat flow, reversing heat flow and non-reversing heat flow. Period=100 s, modulation amplitude=0.2 K and underlying heating rate=3 K/min.

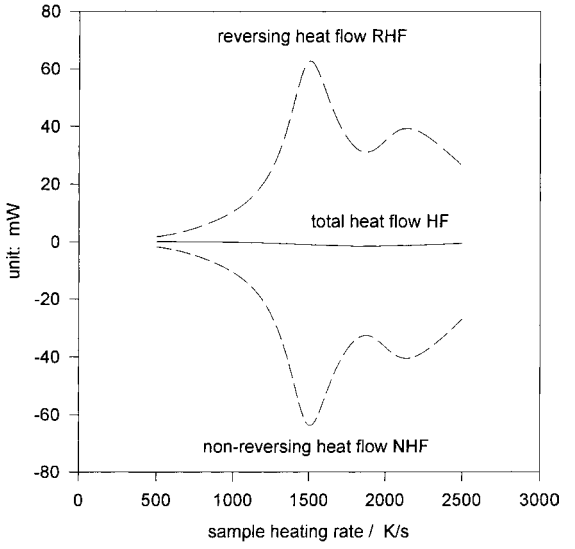

Fig. 5. Simulated total heat flow, reversing heat flow and non-reversing heat flow. Period=1000 s, modulation amplitude=0.2 K and underlying heating rate=3 K/min.

in Figs. 1, 3 and 5. As can be noted, the decomposition takes approximately 2000 s to complete with an underlying heating rate of 3 K/min, hence it can be thought of as a comparatively slow and mild reaction. (As should be mentioned, not all kinetic events have such a long duration). There are several dozen modulation cycles during the decomposition. According to Eqs. (6b) and (9a), due to the fast modulation frequency, we know that the contribution of the kinetic part to the observed heat capacity will be relatively small. In this case the obtained reversing heat flow and non reversing heat flow are separated rather satisfactorily.

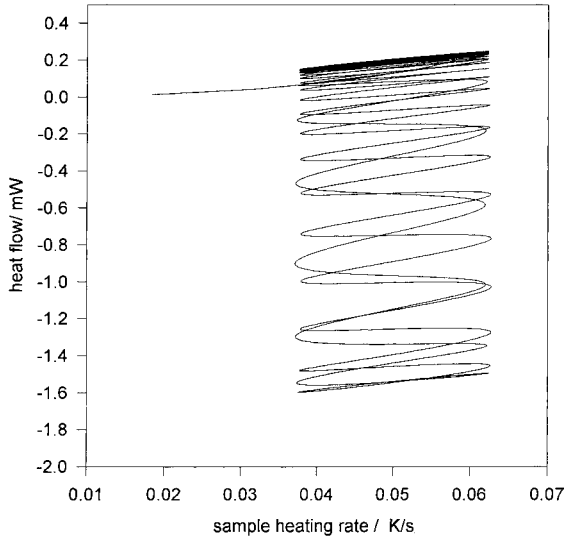

Fig. 4. Simulated Lissajous figure. Period=100 s, modulation amplitude=0.2 K and underlying heating rate=3 K/min.

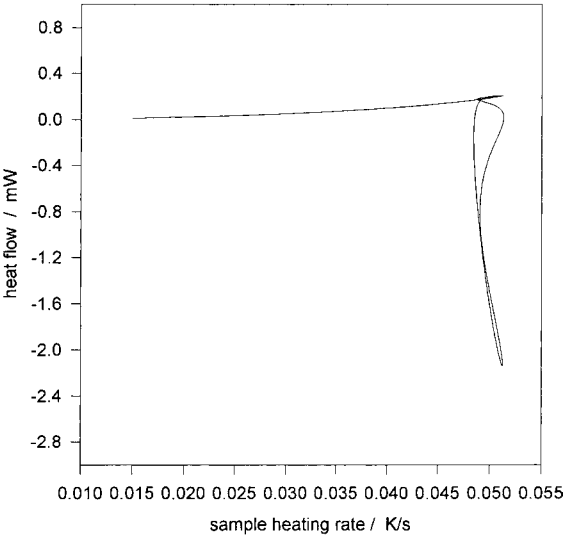

Fig. 6. Simulated Lissajous figure. Period=1000 s, modulation amplitude=0.2 K and underlying heating rate=3 K/min.

With Eq. (14), it is found the maximum value of f'_T during the decomposition is 0.086 mJ/K when the linear heating rate is 3 K/min, hence $(f'_T/\omega C_s)^2_{max} = 0.0012$, which is significantly smaller than one. This satisfies Eq. (10), according to Fig. 1, the error involved is almost negligible. Fig. 2 exhibits the corresponding Lissajous figure. The trace shows an elliptical pattern with small overlap between contiguous modulation cycles, which is an indication of good system linearity in the whole reaction process.

Compared to Fig. 1, the temperature simulation period is 100 s for the simulation shown in Fig. 3, which is increased by a factor of 10. All other parameters are kept the same. The maximum value of $(f'_T/\omega C_s)^2 = 0.12$, which is approximately 100 times larger than that of Fig. 1. Although there are still quite a lot modulation cycles in the decomposition, system linearity begins to be compromised. A much bigger deviation can be expected in the obtained reversing heat flow and non-reversing heat flow. The corresponding Lissajous curve as shown in Fig. 4 deviates from elliptical pattern, showing something similar to an overlapped sine curve. We can infer from that the linearity lost a lot and the system is running into a relatively non-stable status. In Fig. 3, although the total heat flow still looks similar to that of Fig. 1, the deconvoluted reversing heat flow and non reversing heat flow in reaction are markedly different. Maxima are seen up in the reversing heat flow which are only mathematical artifacts. The real reversing heat flow should not change because sample heat capacity remains the same. However, this could lead to incorrect conclusions regarding the sample material properties.

In Fig. 5, the modulation period is increased by another factor of 10–1000 s, less than but reaching the same order as the total decomposition reaction time. (Although this long period is rarely seen in real practice, we just use it here to demonstrate the effect). All other parameters keep the same, however, but in this case $(f'_T/\omega C_s)^2_{max} = 11.8$, increased by another 100 times than that of Fig. 2 and 10,000 times bigger than in Fig. 1. We can no longer assume $f(t, T)$ and f'_T are constant in a modulation cycle, which is a prerequisite for Eq. (4) to be linearized. In this case the kinetic perturbation is too big to be taken as a linear incidence. The corresponding Lissajous figure in Fig. 6 shows the system completely lost linearity and is far from an stable or equilibrium state, which agrees well with the above analysis. The deconvoluted reversing heat flow and the non-reversing one are severely deformed, and even the total heat flow curve has been drastically changed. These data can therefore not provide meaningful information with regard to the sample properties under these circumstances.

Similar results can be obtained from the analysis by Lacey et. al. [20], although their approach is much more complicated and the main point is to explain that it is possible to separate out the contribution to the heat flow which comes from the sample's heat capacity and the part that comes from the non-reversing reaction in many cases.

3. Experimental case analysis, specific heat determination of an amorphous alloy

Fig. 7 is the experimentally determined specific heat, total heat flow, reversing and non-reversing heat flow for a melt spun $Al_{84}Nd_9Ni_7$ ribbon sample (melt spinning speed, 30 m/s), which has an amorphous structure. In the total heat flow curve, there are two exothermic peaks corresponding to the crystallization of aluminum and other inter-metallic compounds, respectively. The TMDSC experiment was carried out with a TA Instruments MDSC 2920 unit using a liquid nitrogen cooling system. The sample size was 13.00 mg, the modulation amplitude 0.8 K, the period 30 s, and the underlying heating rate 1 K/min.

The specific curve can be roughly divided into three distinct major stages (the dotted guide lines are used to help explain the specific heat difference). First is the amorphous stage, segment AB, which has a random atomic arrangement, exhibits the highest C_p profile. The second stage, segment CD, after the first crystallization peak but before the second one, has a partially crystallized amorphous structure, showing an intermediate C_p profile among segments AB, CD and EF. Last is segment EF, which has a fully crystallized structure, and demonstrates the lowest specific heat capacity. Although specific heat difference between crystalline and amorphous states is rather small, TMDSC shows high sensitivity that allows the operator to distinguish them in a single run.

When one looks at the crystallization segments BC and DE, it can be noticed that the first crystallization

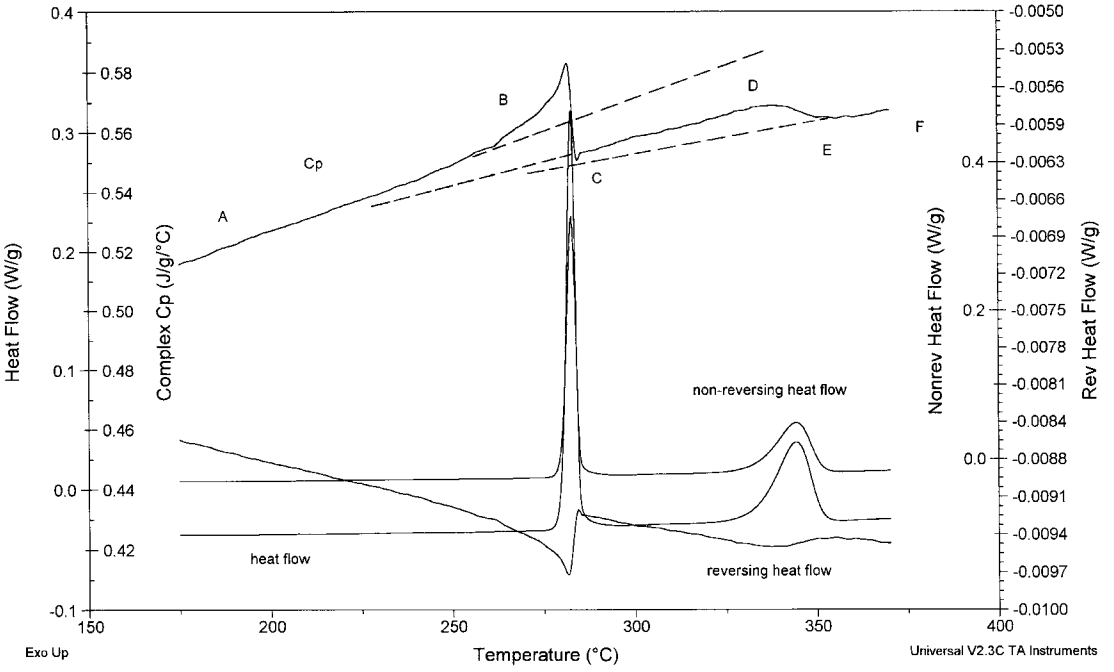

Fig. 7. Experimentally obtained sample specific heat, heat flow, reversing and non-reversing heat flow. Sample material: melt spun $Al_{84}Nd_9Ni_7$ amorphous ribbon. Period=30 s, amplitude=0.8 K, underlying heating rate=1 K/min and sample size=13.00 mg.

peak is relatively sharp and narrow compared with the second one, and the C_p curve shows different pattern during these two transitions. Between BC, C_p exhibits considerable positive deviation, reaching a maximum during the crystallization and then drops sharply as heating goes on. In segment DE, however, the C_p curve transfers smoothly to the fully crystallized segment EF without apparent excessive specific heat peak.

The Lissajous figures for the two crystallization processes are given in Figs. 8 and 9. In Fig. 8, the temperature range is selected to be from 260 to 290°C (corresponding to the first peak), while in Fig. 9, the range shown is from 330 to 360°C (for the second peak). The derivative modulated temperature versus the modulated heat flow curve in Fig. 8 shifted considerably in the vertical direction during the crystallization. Apparently, the linearity shown in Fig. 8 is not as good as that in Fig. 9, in which the Lissajous curve is composed of a slightly shifting ellipse, very similar to the curve pattern in the computer simulation as shown in Fig. 2. Besides, from the shape of the two peaks in the total heat flow curve, it can be shown that the temperature sensitivity f'_T for the first peak should be much bigger than the second one, thus the kinetic heat flow $f(t, T)$ may not be assumed a constant in each of its modulation cycle for the first crystallization. This linearity difference together with Eq. (10) can help explain the different C_p pattern of the two transitions peaks.

In Fig. 10, the specific heat capacity, heat flow, reversing and non-reversing heat flow obtained from a second sample (sample size 13.20 mg) are presented. The difference is in the underlying heating rate, which was reduced from 1 to 0.5 K/min, thus, to lower the crystallization peak intensities and accommodate more modulation cycles. This has a similar effect to increasing modulation frequency but without remarkably affecting the calibration factor as does frequency. Modulation period and amplitude were kept unchanged. The C_p curve shows much smaller excessive value at the first crystallization peak, and still goes smoothly at the second transition. The Lissajous figures of the same temperature ranges as the first sample (260–290°C and 330–360°C) are given in Figs. 11 and 12, accordingly, both showing improved linearity over the first sample run.

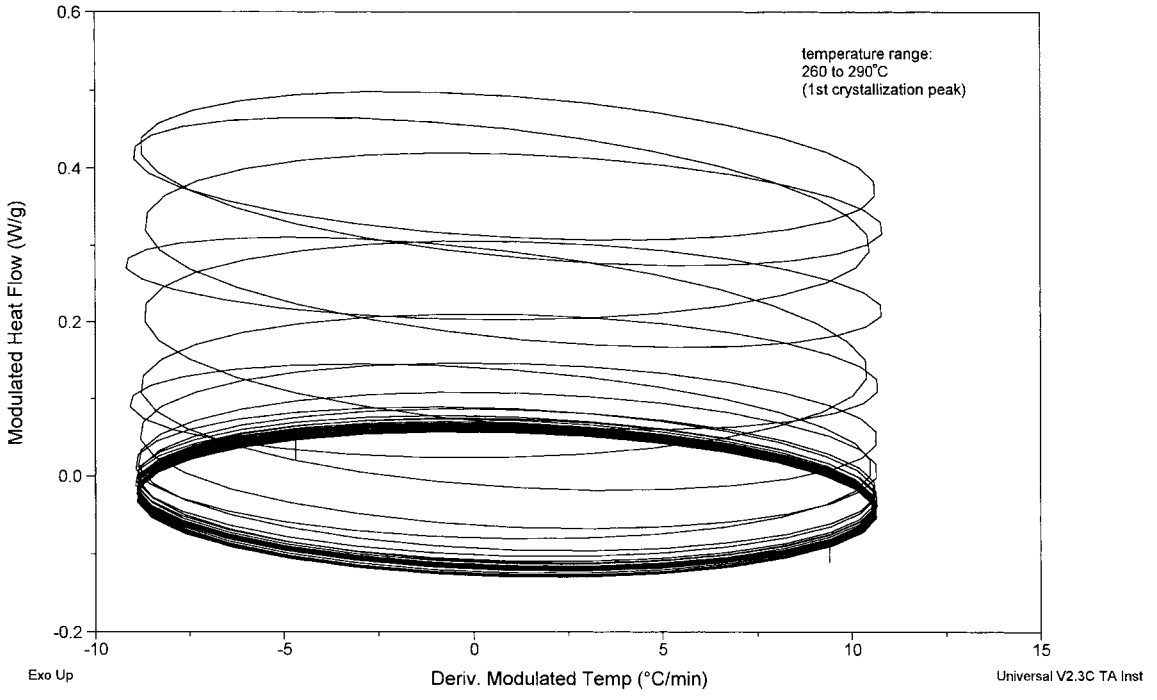

Fig. 8. Lissajous figure for the first crystallization peak in Fig. 7. Temperature range: 260–290°C. Period=30 s, amplitude=0.8 K, underlying heating rate=1 K/min and sample size=13.00 mg.

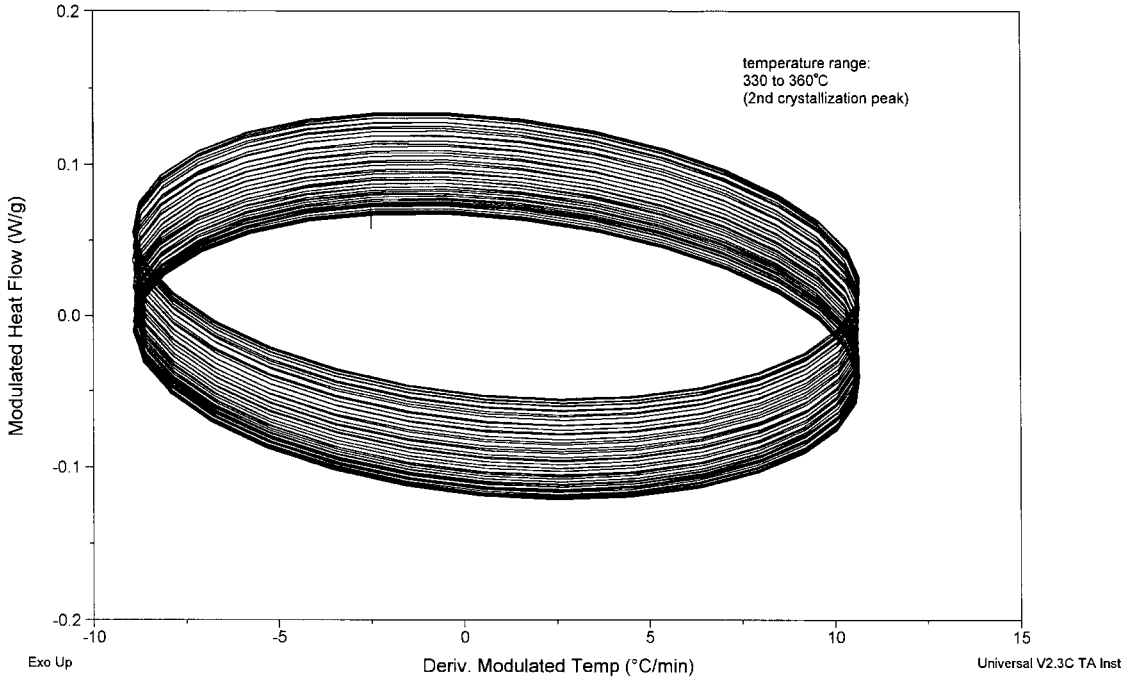

Fig. 9. Lissajous figure for the second crystallization peak in Fig. 7. Temperature range: 330–360°C. Period=30 s, amplitude=0.8 K, underlying heating rate=1 K/min and sample size=13.00 mg.

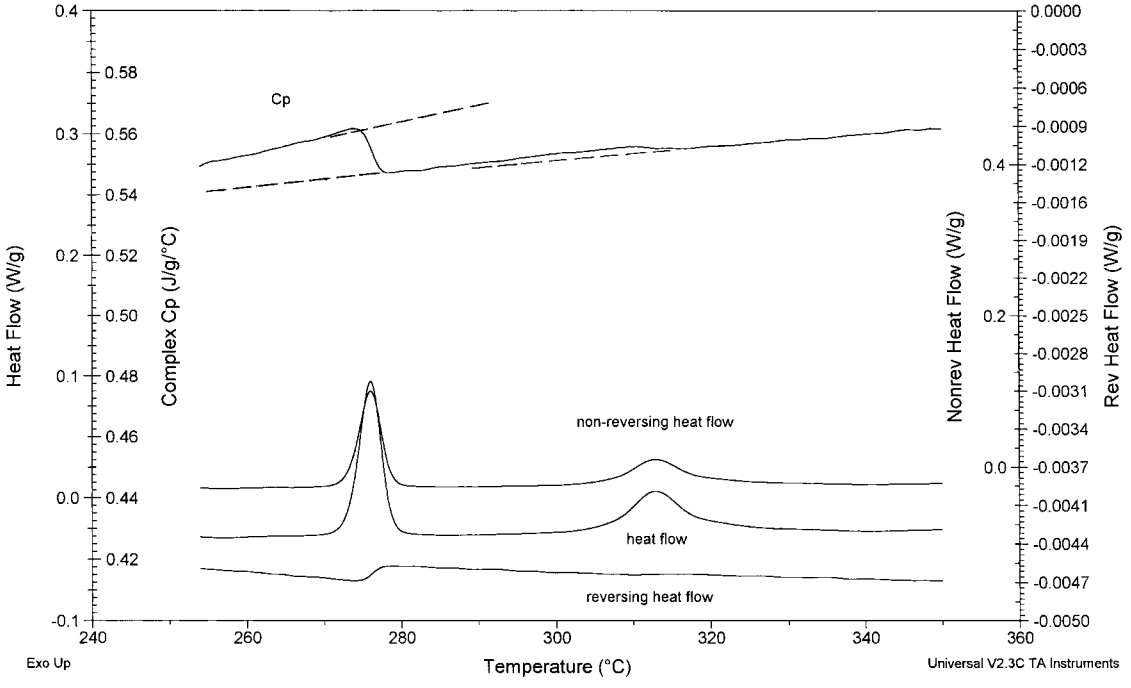

Fig. 10. Experimentally obtained sample specific heat, heat flow, reversing and non-reversing heat flow. Period=30 s, amplitude=0.8 K,underlying heating rate=0.5 K/min and sample size=13.20 mg.

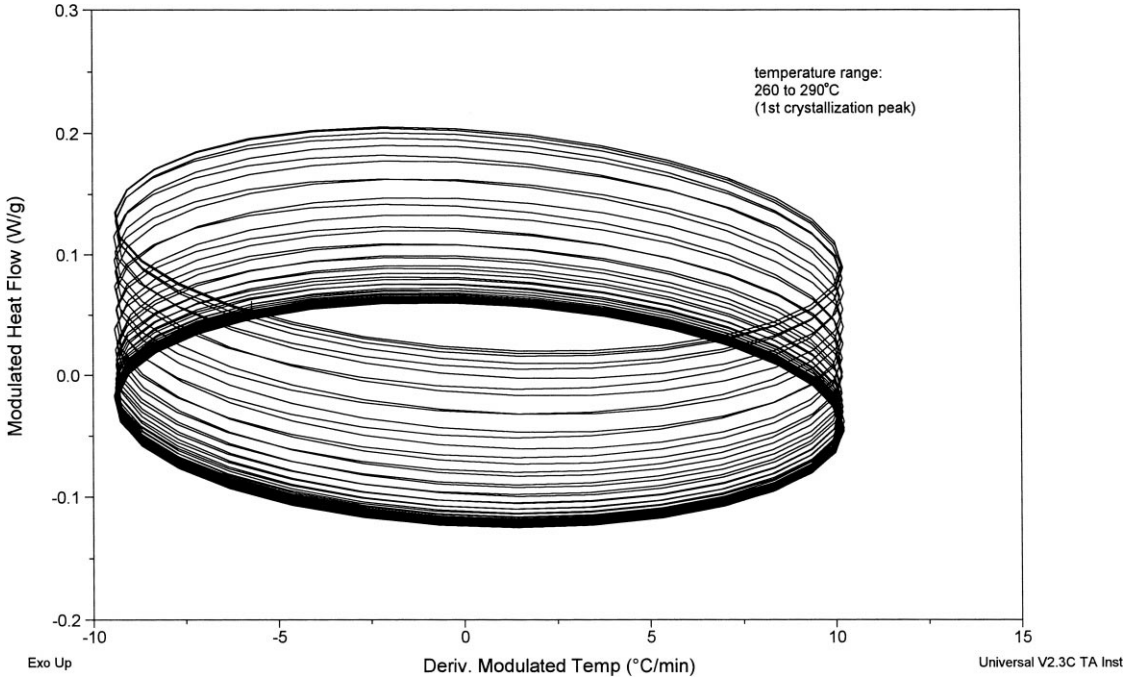

Fig. 11. Lissajous figure for the first crystallization. Temperature range: 260–290°C. Period=30 s, amplitude=0.8 K, underlying heating rate=0.5 K/min and sample size=13.20 mg.

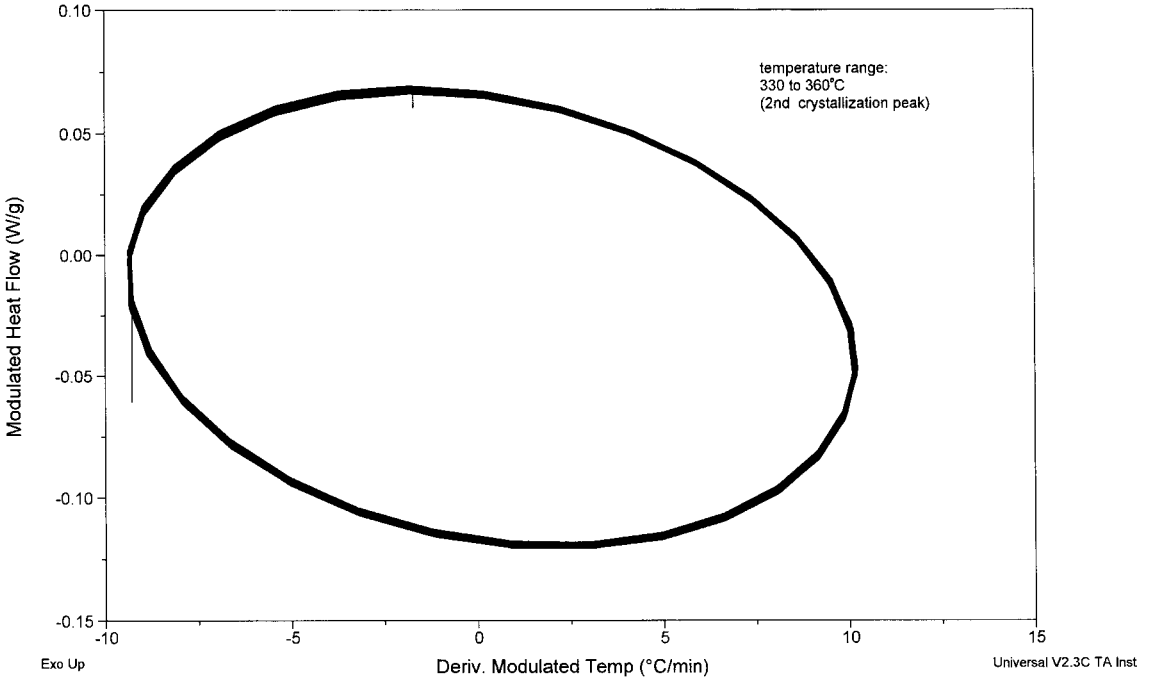

Fig. 12. Lissajous figure for the second crystallization. Temperature range: 330–360°C. Period=30 s, amplitude=0.8 K,underlying heating rate=0.5 K/min and sample size=13.20 mg.

4. Experimental parameter selection considerations

It has been demonstrated that kinetic events can affect the observed specific heat. Based on the above analytical equations, numerical simulations and experimental results, it can be seen that in order to really apply the power of TMDSC, the key is to make the test process take place under a linear or close to linear conditions. At least some measures can be taken to make this more likely to occur.

Use a lower underlying heating rate, hence if the kinetic reaction is time and temperature dependent, it will take a longer time to complete, this will effectively reduce f_T'.

Use a small modulation amplitude, accordingly, the perturbation introduced will be lower too, thus the linearity could be improved accordingly.

Use a relatively high modulation frequency, this together with Eq. (1) can generate more cycles in kinetic event. However, increasing the temperature modulation frequency is subject to some physical limitations. Firstly due to the thermal latency of the instrument itself, commercially available TMDSC equipment has a very narrow dynamic range, say, 0.1–0.01 Hz, which is much smaller than some other dynamic evaluation methods. Fortunately, the modulation frequency range problem could be overcome by the latest development in light modulated TMDSC [21,22]. Besides, use of a high modulation frequency can introduce extra temperature gradient and phase lags for poor thermally conducting materials, which will make the results extremely difficult to analyze quantitatively unless a much smaller sample size is used. It has been found that the sample specific heat obtained from TMDSC at the high frequency spectrum deviates a lot even after calibration factors have been taken into account [23]. Finally, sharp, intense kinetic event can have a major effect on the observed sample specific heat and generate spurious artifacts, while a broad and gentle kinetic reaction is more favorable to the quantitative separation of reversing heat flow and non reversing flow with TMDSC [24,25]. All these can make the situation complicated, thus careful parameter selection and result explanation is important when using TMDSC.

5. Conclusions

TMDSC has certain merits over conventional DSC, but the complications involved with the linear system response and small kinetic perturbation requirement makes this method limited in quantification of kinetic events under some situations. Care must be taken in terms of the experimental parameters selection and results explanation. Through simulation and experiments, several items have been demonstrated that can help improve overall linearity and reduce the test errors.

References

[1] P.S. Gill, S.R. Saurbrunn, M. Reading, J. Therm. Anal. 40 (1993) 931–939.
[2] M. Reading, Trends Poly. Sci. 8 (1) (1993) 248–253.
[3] M. Reading, D. Elliot, V.L. Hill, J. Therm. Anal. 40 (1993) 949–955.
[4] B. Wunderlich, Y. Jin, A. Boller, Thermochim. Acta 238 (1994) 277–293.
[5] M. Reading, A. Luget, R. Wilson, Thermochim. Acta 238 (1994) 295–307.
[6] M. Song, A. Hammiche, H.M. Pollock, D.J. Hourston, M. Reading, Polymer 36 (1995) 3313–3316.
[7] M. Wuff, M. Alden, Thermochim. Acta 256 (1995) 151–165.
[8] J.E.K. Schawe, G.W. Hohne, J. Therm. Anal. 46 (1996) 893–903.
[9] N.J. Coleman, D.Q.M. Craig, Int. J. Pharmaceut. 135 (1996) 13–29.
[10] F. Roussel, J.M. Buisine, J. Therm. Anal. 47 (1996) 715–725.
[11] I. Okazaki, B. Wunderlich, Macromolecules 30 (1997) 1758–1764.
[12] A. Toda, M. Hikosaka, Y. Saruyama, Thermochim. Acta 293 (1997) 47–63.
[13] B. Wunderlich, Thermal Analysis, Academic Press, Boston, 1990 (Chapter 4).
[14] R. Sherrenberg, V. Mathot, P. Steeman, J. Therm. Anal. 54 (1998) 477–499.
[15] I. Hatta, N. Katayama, J. Therm. Anal. 54 (1998) 577–584.
[16] F.U. Buehler, C.J. Martin, J.C. Seferis, J. Therm. Anal. 54 (1998) 501–519.
[17] H. Baur, B. Wunderlich, J. Therm. Anal. Calorim. 54 (2) (1998) 437–465.
[18] M. Reading, R. Luyt, J. Therm. Anal. 54 (1998) 535–544.
[19] S. Weyer, A. Hensel, C. Schick, Thermochim. Acta 304/305 (1997) 267–275.
[20] A.A. Lacey, C. Nikolopoulos, M. Reading, J. Therm. Anal. 50 (1997) 279–333.
[21] T. Ozawa, K. Kanari, J. Therm. Anal. 54 (1998) 521.
[22] T. Ozawa, K. Kanari, J. Therm. Anal. Calorim. 56 (1999) 691.
[23] B. Schenker, F. Stager, Thermochim. Acta 304/305 (1997) 219.
[24] M.L.D. Lorenzo, B. Wunderlich, J. Therm. Anal. 57 (1999) 459–472.
[25] S.X. Xu, Y. Li, Y.P. Feng, Thermochim. Acta 343 (2000) 81–88.